Volume 21, No 3 | International Journal of Radiation Research, July 2023

Significance of magnetic resonance zoomed imaging with parallel transmission intravoxel incoherent motion imaging, ultrasonography and dual-energy computed tomography imaging in the differential diagnosis of benign thyroid nodule and papillary thyroid carcinoma

Y. He[1#*], X. Qi[1#], X. Luo[1], W. Wang[1], H. Yang[1], M. Xu[1], X. Wu[1], W. Fan[2]

[1]Department of Radiology, Ma'anshan People's Hospital, Maanshan, Anhui, 243000, China
[2]School of graduate, Wan'nan Medical College, Wuhu, 241000, China

► ***Original article***

***Corresponding author:**
Yongsheng He, Ph.D.,
E-mail:
yongshenghe1431@163.com

Received: March 2022
Final revised: August 2022
Accepted: August 2022

Int. J. Radiat. Res., July 2023; 21(3): 537-543

DOI: 10.52547/ijrr.21.3.25

Keywords: *Papillary thyroid carcinoma, benign thyroid nodules, ZOOMit IVIM imaging, ultrasonography, dual-energy CT imaging.*

#these authors contributed equally to this study.

ABSTRACT

***Background*:** To assess the use of computed tomography (CT), ultrasonography and magnetic resonance imaging (MRI) in distinguishing papillary thyroid cancer (PTC) from benign thyroid nodules. ***Materials and Methods*:** A total of 45 cases with benign thyroid nodules and 75 cases with papillary thyroid cancer were included from our hospital from March 2020 to December 2021. All patients were examined by MRI, ultrasonography and dual-energy CT. The outcomes of the two groups' MRI, CT and ultrasonography scans were compared. ***Results*:** The benign nodule group had significantly higher pure diffusion coefficient (D) (1.38±0.32 vs 0.95±0.12), perfusion fraction (F) values (17.13±4.35 vs 12.83±2.93) and iodine concentration (IC) plain scan scores (0.96±0.44 vs 0.56±0.37), whereas it had lower IC artery scores (2.65±1.11 vs 3.92±1.22) than those of the PTC group ($p<0.001$ for all). The Emax value of the PTC group was substantially greater than that of the benign nodule group (62.53±37.93 vs 25.37±8.38, $p<0.001$), and the percentage of nodules with aspect ratio ≥ 1 was higher in the PTC group than in the benign nodule group (48.0% vs 22.2%, $p=0.005$). The area under the curve (AUC) for MRI in the diagnosis of PTC patients was 0.885, which was substantially higher than those for ultrasonography (AUC=0.705) and CT exams (AUC=0.753) ($p<0.001$). ***Conclusion*:** MRI, ultrasonography and CT examinations are essential for discriminating between benign thyroid nodules and PTC. MRI has better diagnostic accuracy than the other two tests.

INTRODUCTION

The prevalence of thyroid nodules, a common thyroid condition, is now rising yearly. Thyroid cancer accounts for 7%–15% of thyroid nodules, of which more than 90% are differentiated thyroid carcinoma, such as papillary thyroid cancer (PTC) [1]. Studies showed that China had a 19%–67% detection rate for thyroid nodules, and most thyroid nodules are benign (mainly nodular goitres), with malignant nodules accounting for 30% [2]. The primary approach for treating malignant thyroid nodules is surgery. For clinical therapy, surgical procedure selection and prognosis, the early diagnosis and correct identification of benign and malignant nodules are crucial [3]. Therefore, an accurate imaging assessment of thyroid nodules is required preoperatively.

Currently, ultrasonography is the preferred imaging examination technique for identifying thyroid neoplasms as its differential diagnosis has greater than 85% accuracy. However, there are still limitations in examining the relationship between tiny lesions, lesions and the surrounding trachea and oesophageal mucosa, and it is affected by the operator's subjective probe compression, which changes the aspect ratio of thyroid tumours. Therefore, its differential diagnostic accuracy varies greatly [4]. Additionally, it has been observed that the existing thyroid nodule malignancy risk categorisation methods based on ultrasonography are ineffective at detecting follicular tumours [5].

Existing studies have shown that computed tomography (CT) and magnetic resonance imaging (MRI) are commonly used imaging methods for diagnosing thyroid neoplasms. These two methods are conducive to observing the structure of the lesion and its spatial relationship with the surrounding tissues, especially in assessing the infiltration of the lesion to adjacent tissues and cervical lymph node metastasis [6, 7]. According to a previous study, the differential diagnosis of complicated, tiny and primarily concealed haemorrhagic nodules from recent bleeding may benefit from the molecular

[DOI: 10.61186/ijrr.21.3.537]

information supplied by spectral dual-energy computed tomography (DECT) [8]. CT examinations have good imaging effects on anatomical structures but have ionising radiation.

High soft tissue resolution and no radiation are two benefits of MRI, which may properly represent both the functional information and the anatomical structure of the tissue. There is currently little evidence on the qualitative diagnosis of thyroid nodules by MRI in China, and those that do exist are restricted to the morphology-based identifications of illnesses. By quantitatively evaluating the diffusion and microvascular perfusion properties of tissues, intravoxel incoherent motion (IVIM) diffusion-weighted imaging (DWI) may give complete information for thyroid nodule identification [9]. The zoomed imaging with parallel transmission (ZOOMit) technique based on the parallel transmitting platform uses a small field of vision to selectively excite the region of interest (ROI), and there is no radio frequency interference between the obtained image levels, thereby reducing image blur and distortion. ZOOMit DWI makes up for the deficiency of conventional DWI technology in thyroid examination, especially for small organ lesions [10]. MRI has obvious advantages in thyroid examination, but the cost is high.

Considering the benefits and drawbacks of the aforementioned imaging techniques, this study was conducted to compare further the impact of various imaging techniques on the diagnostic accuracy of thyroid nodules and on PTC patients. We used MRI (ZOOMit DWI), ultrasonography and dual-energy CT imaging to preliminarily explore its differential diagnosis value in patients with thyroid nodules and PTC and provide evidence for clinical practice.

MATERIALS AND METHODS

General information

From March 2020 to December 2021, patients with benign thyroid nodules and PTC as confirmed by surgery and pathology were retrospectively enrolled from Ma'anshan People's hospital. Inclusion criterion: thyroid nodules could be observed and measured completely and effectively on MRI images. Exclusion criterion: postoperative pathology showed that patients had two or more thyroid nodules. All patients signed informed consent, and the ethics committee approved the study.

Study method

This was a retrospective study where 120 patients with benign thyroid nodules and PTC underwent MRI, ultrasonography and dual-energy CT examination, aiming to compare the diagnostic accuracy of these three imaging diagnostic tools in the discrimination of benign thyroid nodules and PTC (figure 1).

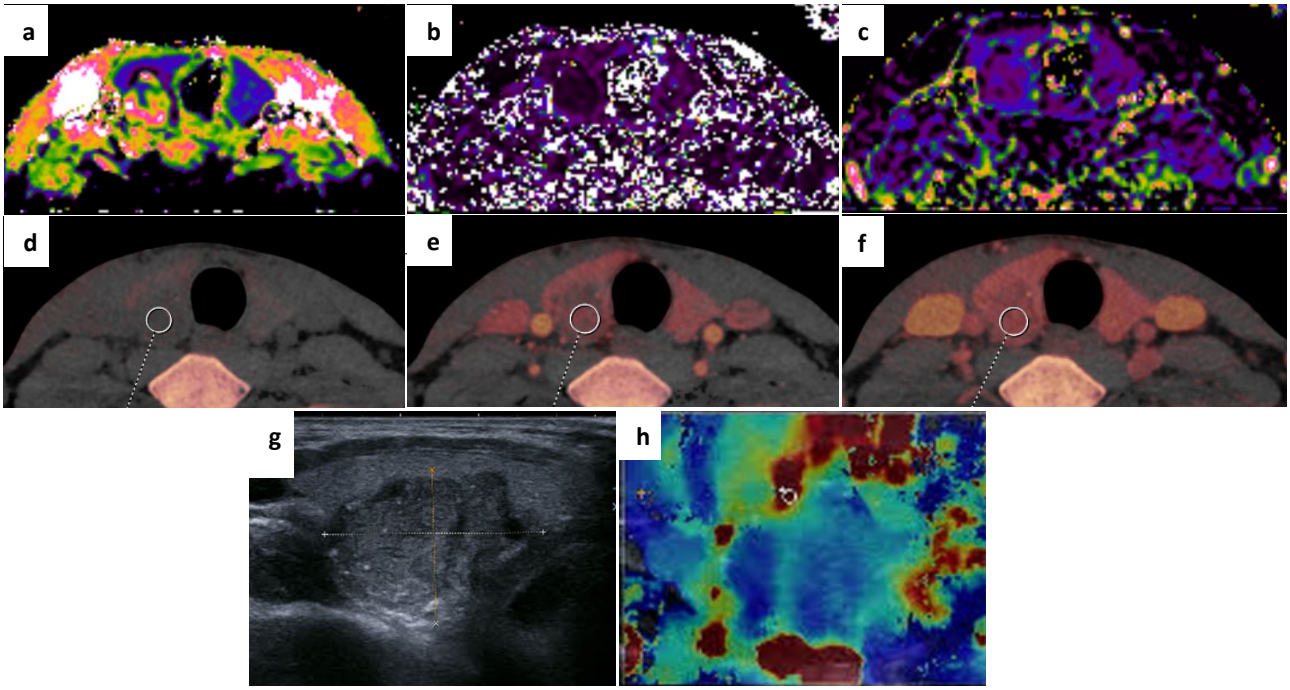

Figure 1. A 39-year-old male patient presented with papillary carcinoma of the right lobe of the thyroid with a mass size of about 3.2cm×1.7cm×1.5cm, which involved the thyroid capsule. **(a)** pure diffusion coefficient **(D)** pseudo-color maps; **(b)** pseudo-diffusion coefficient **(D*)** pseudo-color maps; **(c)** perfusion fraction **(F)** pseudo-color maps; **(d)** IC plain scan; **(e)** IC artery; **(f)** IC vein; **(g)** two-dimensional ultrasound; **(h)** elastography.

[DOI: 10.61186/ijrr.21.3.537]

Magnetic resonance imaging examinations and findings

A 3.0 T superconducting MR imager (Siemens MAGNETOM Prisma, Germany) was used in combination with a 64-channel head/neck coil and 8-channel neck surface coil (Zhongzhi, China) for examination. The patient was asked to take the supine position, their neck was elevated, and the thyroid was fully exposed. The neck was scanned routinely. During the scanning process, the patient was asked to avoid swallowing. Scanning sequences included a cross-sectional T1 weighted image (T1WI) and ZOOMit IVIM DWI. (1) T2WI: repetition time (TR) 3030 ms, time to echo (TE) 81 ms, field of view (FOV) 240 mm × 180 mm, slice thickness 4 mm, scanning time 2 min 7 s; (2) ZOOMit IVIM： small FOV. With the thyroid structure as the centre, the size was 120 mm × 62 mm, TR 3600 ms, TE64 ms, FOV layer thickness was 4 mm, b values were 0, 40, 80, 120, 160, 200, 400, 600, 800, 1000 and 2000 s / mm^2.

IVIM data processing uses medical imaging interaction toolkit software (Version2011, DKFZ, Heidelberg, Germany), and the obtained parameters included the pure diffusion coefficient (D), pseudo-diffusion coefficient (D*) and perfusion fraction (F) pseudo-colour maps. D represents molecules' true diffusion coefficient information, also known as ADC slow. F is the perfusion fraction, which refers to the volume ratio of microcirculation perfusion in the voxel to the total diffusion effect, reflecting blood flow information. D* represents microcirculation within the voxel and is perfusion-related diffusion, also known as ADC Fast. The ROI was manually delineated on the integration toolkit SAP software with b = 600 DWI images. Three measurements of the D, D* and F values were made, and the average value was computed. The ROI's size during the diagnostic procedure was set at 20–35 $mm^{2,}$ and areas of haemorrhage, necrosis, calcification or cystic degeneration were avoided as much as possible during the ROI's setting. Comparisons were made between the D, D* and F values of the two patient groups.

Computed tomography examinations and findings

A standard neck scan that included the area from the base of the skull to the aortic arch was conducted using a third-generation DECT scanner (Siemens SOMATOM, Germany) before imaging capture. Dual-energy scanning modes: 128 × 0.6 mm detector arrangement; 0.5 s gantry rotation; and 0.7 tone factor. The A-tube operated at the peak voltage of 100 keV and the current at 118 mA. The B-tube operated at the peak voltage of Sn 140 keV and the current at 178 mA. The matrix was 512 × 512, FOV was 25 × 25 cm, pitch was 0.8 mm, slice thickness was 6 mm and reconstructed image slice thickness was 0.8 mm. An automated high-pressure syringe was used to provide the non-ionic iodide contrast agent (Ioversol, Hengrui Medicine, Jiangsu, China) at a flow rate of 3.5 ml/ s for a total of 50 to 75 ml (the total amount of injection was adjusted according to the height and weight of the patient). Dual-energy contrast-enhanced scanning was performed after a parallel sweep and, with a dosage of 1 ml/ kg body weight, Ioversol (320 mg/ ml) was given intravenously via the elbow at a rate of 3.0 ml/ s using a double-tube high-pressure syringe. After injection of the contrast agent, 30 ml of normal saline was injected. Afterwards, there was a delayed 25 s action pulse dual energy scan and a venous phase dual energy scan after 60 s.

Two radiologists retrospectively read the cross-sectional images of CT examination without knowing the pathological results, and the opinions were determined by negotiation at the same time. Iodine levels were measured in thyroid nodules' arterial, venous and plain scan phases, which were recorded as iodine concentration (IC) plain scan, IC artery and IC vein, respectively.

Ultrasonography examinations and findings

Shear wave elastography (SWE) was performed using the Supersonic Aixplorer color Doppler ultrasonography diagnostic instrument (Supersonic Imagine, France). A linear array probe was used, and the probe frequency was 4–15 MHz. After finding thyroid nodules by conventional ultrasonography, the SWE mode was commenced. SWE elastic imaging technology examined malignant thyroid nodules: Young's modulus Emax, kappa. Ultrasonography measurement parameters included the size, aspect ratio, calcification and E max value.

The two groups' maximum diameter, calcification, aspect ratio, capsule and Emax values as measured by SWE were compared.

Statistical analysis

SPSS version 26.0 was utilised for the statistical evaluation. The mean and standard deviation of the quantitative data that followed a normal distribution were utilised to characterise the data, and an independent sample t-test was used for comparison analysis. The chi-square test was utilised for comparison analysis, and qualitative data were presented as n (%) values. The area under the curve was calculated using the receiver operating characteristic curve to assess the diagnostic effectiveness of MRI, ultrasonography and CT exams in PTC patients. A statistically significant difference was indicated by $p < 0.05$.

RESULTS

A total of 45 patients with benign thyroid nodules were included. These included 27 patients with nodular goitre, 13 patients with thyroid adenoma and five patients with chronic lymphatic thyroiditis. Their

[DOI: 10.61186/ijrr.21.3.537]

ages ranged from 27 to 86, with an average age of 54.4 ± 10.3 y. There were 12 men and 33 women. Additionally, 75 PTC patients were also included. Their ages ranged from 16 to 71, with an average age of 49.6 ± 11.4 y. There were 11 men and 64 women. There was no significant difference in baseline between the two groups ($p > 0.05$) with the exception of the illness course and nodule morphology ($p < 0.001$) (table 1).

Table 1. Basic information of benign nodule and PTC group.

Group	benign nodule (n=45)	PTC(n=75)	t/x2	p
Gender (male/ female)	12/33	11/64	2.614	0.106
Age (year)	54.4±10.3	49.6±11.4	-2.348	0.225
BMI	24.15±6.18	21.41±3.08	-0.701	0.487
Course of disease (month)	2.96±2.01	1.31±0.75	-5.283	<0.001
Nodules form			19.200	<0.001
Solid nodules	10(22.22%)	74(98.67%)		
Cystic solid nodules	35(77.78%)	1(1.33%)		

Note: PTC: papillary thyroid carcinom; BMI: Body Mass Index.

Analysis of magnetic resonance zoomed imaging with parallel transmission intravoxel incoherent motion imaging examinations between the two groups

As shown in table 2, the D and F values in the benign nodule group were higher than those in the PTC group (1.38 ± 0.32 vs 0.95 ± 0.12; 17.13 ± 4.35 vs 12.83 ± 2.93), and the difference was statistically significant ($p < 0.001$). The D* value, however, was significantly lower than that in the PTC group (12.23 ± 5.76 vs 15.59 ± 4.08, $p < 0.001$).

Table 2. Analysis of MRI ZOOMit IVIM between benign nodule and PTC group.

	benign nodule (n=45)	PTC(n=75)	*t*	*P*
D ($10^{-3}mm^2/s$)	1.38±0.32	0.95±0.12	-10.595	<0.001
D*($10^{-3}mm^2/s$)	12.23±5.76	15.59±4.08	3.729	<0.001
F (%)	17.13±4.35	12.83±2.93	-6.465	<0.001

Analysis of computed tomography examinations between the two groups

The IC plain scan of the benign nodules group in the CT examination was greater than the PTC group (0.96 ± 0.44 vs 0.56 ± 0.37, $p < 0.001$). When compared to the PTC group, the IC artery was substantially smaller (2.65 ± 1.11 vs 3.92 ± 1.22, $p < 0.001$). As demonstrated in table 3, there was no discernible change in the IC vein between the two groups (2.50 ± 1.19 vs 2.94 ± 1.19, $p < 0.001$).

Table 3. Analysis of CT examination between benign nodule and PTC group.

index	benign nodule(n=45)	PTC(n=75)	*t*	*P*
IC plain scan	0.96±0.44	0.56±0.37	-5.404	<0.001
IC artery	2.65±1.11	3.92±1.22	5.725	<0.001
IC vein	2.50±1.19	2.94±1.19	1.937	0.055

Note: PTC: papillary thyroid carcinom; IC: iodine concentration

Comparison of ultrasonography examinations between the two groups

In ultrasonography, there was a significant difference in the aspect ratio and Emax value of the nodules between the two groups ($p < 0.001$). The PTC group had a significantly higher proportion of nodules with an aspect ratio ≥ 1 (48.0% vs 22.2%, $p = 0.005$) and Emax value (62.53 ± 37.93 vs 25.37 ± 8.38, $p < 0.001$) than those in the benign nodules group, as shown in table 4.

Table 4. Comparison of ultrasonography between benign nodule and PTC group.

index	category	Benign Nodule (n=45)	PTC(n=75)	*t*	*P*
Maximum diameter		1.38±0.70	1.32±0.92	-0.376	0.707
Calcification					
	with	28(62.2)	48(64.0)	0.038	0.845
	without	17(37.8)	27(36.0)		
Aspect ratio					
	≥1	10(22.2)	36(48.0)	7.906	0.005
	<1	35(77.8)	39(52.0)		
Capsule					
	with	12(26.7)	10(13.3)	3.340	0.068
	without	33(73.3)	65(86.7)		
Emax		25.37±8.38	62.53±37.93	6.467	<0.001

Note: PTC: papillary thyroid carcinom

Comparison of the diagnostic efficacy of magnetic resonance imaging, ultrasonography and computed tomography examinations for papillary thyroid cancer

As indicated in table 5 and figure 2, the sensitivity and specificity of MRI in the diagnosis of PTC were considerably greater than those of ultrasonography and CT ($p < 0.001$).

Table 5. Comparison of the diagnostic efficacy of MRI, ultrasonography and CT examinations in PTC.

Method	MRI (D)	Ultrasonography	CT	P
Sensitivity	87.36%	82.57%	83.43%	<0.001
Specificity	80.63%	70.47%	75.58%	<0.001
AUC	0.885	0.705	0.753	<0.001
AUC (95%CI)	0.806~0.923	0.543~0.725	0.624~0.867	-

Note: MRI: magnetic resonance imaging; PTC: papillary thyroid carcinoma; AUC: the area under the curve

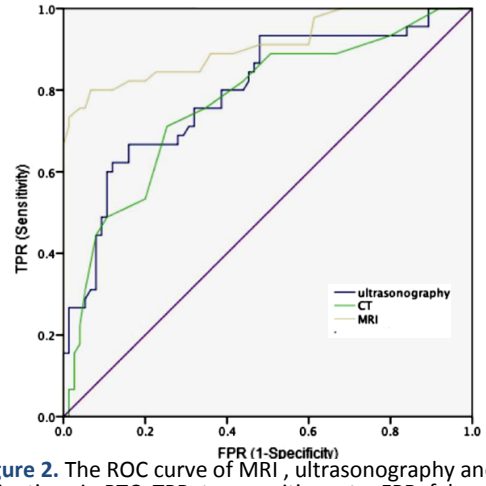

Figure 2. The ROC curve of MRI , ultrasonography and CT examinations in PTC. TPR, true positive rate; FPR, false positive rate; MRI, magnetic resonance imaging ; PTC, papillary thyroid carcinoma; AUC, the area under the curve.

[DOI: 10.61186/ijrr.21.3.537]

DISCUSSION

Because of its quick imaging speed, selective imaging, high image resolution and strong signal uniformity, the ZOOMit IVIM technology was employed in this investigation to detect thyroid nodules. This is of great significance in studying the water molecule diffusion and microcirculation characteristics of different thyroid nodule tissues and providing functional imaging information for diagnosis and differential diagnosis. Compared with the DWI mono-exponential model, IVIM can distinguish the information of vascular microcirculation perfusion (F, D*) and water molecule diffusion (D) by selecting different b values [11]. Compared with conventional DWI, the thyroid images of ZOOMit DWI technology are consistent with their anatomies and have substantial benefits in terms of signal-to-noise ratio and image deformation, which improves the accuracy and repeatability of image measurement parameters [12]. The study's findings demonstrated statistically significant variations in D, D * and F values between the groups with benign thyroid nodules and PTC. In comparison with the PTC group, the D value of the benign nodules group was much greater (1.38 ± 0.32 vs 0.95 ± 0.12), which was similar to the results of Sakamoto. The F value of the benign nodules group was significantly higher than that of the PTC group, suggesting that the average blood flow velocity of benign nodules was slower than that of PTC. Furthermore, compared with the PTC group, the benign nodules group's D * value was much lower. The reason may be that D* is a perfusion-related parameter, while the growth of PTC is slow and the malignant degree is low. The area of the high malignant degree of the tumour depends on the obvious perfusion area, which can be considered as the perfusion of malignant nodules is not obvious. In addition, the vascular changes of nodular goitres are very complex, resulting in complex perfusion, and the thyroid around nodules is confused with vascular tumours. Therefore, the significance of the difference in D* value between benign nodules and PTC for differential diagnosis is still unclear. There are still different conclusions about the value of the IVIM parameters in distinguishing between benign and cancerous thyroid nodules. Tan [13] discovered that the F value had the best diagnostic efficacy for identifying benign and malignant nodules among the IVIM sequence's characteristics. However, this study suggests that the evolution and development of different tissue types of nodules are complex. The papillary carcinoma cells are closely arranged, and the microvessel density, flow velocity and perfusion in nodules are complex and unstable. At present, DWI imaging based on IVIM theory is a new direction in thyroid MRI function research and the consistency and stability of its differential diagnosis results need to be studied further.

Some scholars believe that in ultrasonography, clear boundaries and regular capsules are an important basis for diagnosis, as the halo (clear boundary) is mainly seen in benign thyroid tumours. Generally, the halo's integrity, continuity and uniformity suggest that the tumour is benign [14]. The SWE technology used in this study is a quantitative measurement method. SWE has many advantages, such as real-time and objectivity, compared with the traditional assisted elastography technology. The Q-box analysis software of SWE provides intuitive measurement parameters for evaluating tissue hardness. The soft hardness of the organisation is directly reflected by the E max of the Young's modulus. At the same time, the SWE technology generates an acoustic radiation force through the high-speed excitation pulse emitted by the probe so that the organisation vibrates and is quickly captured by the probe, realising the palpation of acoustic waves. SWE avoids the subjectivity of traditional elastic imaging technology [15]. Due to different histological structures, the hardness of the thyroid nodules is also different. Pathological studies show that cancer cells are infiltrating and growing in the tissue and the proliferation of interstitial fibrous tissue in malignant tumour tissue is disordered, so the tissue hardness increases [16]. SWE may be used for the differential diagnosis of thyroid benignity to distinguish between benign and malignant tissue lesions based on this pathological foundation. Patients in this research had an aspect ratio under 1, suggesting that patients with such tumours had less infiltration in surrounding tissues. To increase the effectiveness of early clinical thyroid carcinoma diagnosis, ultrasonography can be utilised based on degrees of differential diagnosis of the patient's maximum diameter of nodules, aspect ratio and tissue softness and hardness due to the indicators of benign nodules and PTC patients displaying significant differences. Through ultrasonography, the appearance of local lesions can be analysed. There are still many shortcomings in SWE detection. For example, calcifications and cystic changes in the thyroid will affect the evaluation of nodule hardness, which often results in its misjudgement [17].

CT is often utilised in detecting thyroid disorders because of the thyroid's excellent natural comparison. When thyroid tissue is diseased, the iodine storage cells are destroyed, and the iodine content in the diseased tissue decreases, forming a low-density area on the CT image. This makes CT scanning one of the effective methods for examining thyroid lesions. Conventional thin-layer plain and enhanced CT scanning is conducive to the display of lymph nodes and their surrounding structures, but it is often unable to be accurately characterised. Dual-energy correlation technology has been utilised extensively to differentiate between benign and

[DOI: 10.61186/ijrr.21.3.537]

malignant thyroid nodules [18], but there are few reports of it being used to identify cervical lymph node metastasis in PCT patients. Dual-source CT has increasingly been used in recent years to determine whether thyroid nodules are benign or cancerous. To discriminate between various compounds, the diagnosis is based on how different substances' absorption capacities vary as the X-ray energy changes. After image post-processing, the iodine map may be generated by separating the iodine-containing materials from the tissue [19]. The dual-energy iodine map may, directly and indirectly, depict the lesion's varying IC and its corresponding blood supply. After image post-processing, the iodine content of the lesion may be quantitatively evaluated, which enhances the sensitivity and accuracy of the diagnosis to some amount [20]. According to the study's findings, there were statistically significant differences between the benign nodules and PTC groups in terms of IC plain scan and IC artery. Among them, the benign nodules group's IC scan score was greater than the PTC group's, which was consistent with the findings of other studies. Li reasoned that the IC scans of malignant thyroid nodules were lower than those of benign nodules because thyroid follicular cells in malignant nodules were less capable of absorbing iodine than those in benign nodules, and cancer cells are incapable of absorbing iodine. The IC scans of PTC were lower than those of benign nodules because it was analogous to malignant nodules [21]. The IC artery of the PTC group in this investigation was greater than that of the benign nodules group. The difference in arterial phase blood flow between PTC and benign nodules was likely the cause. Because the IC artery of the PTC group was greater than that of the group with benign nodules, it has been suggested that the IC artery may be a more objective metric for assessing PTC patients.

This research still has a number of shortcomings, including: 1. for the retrospective study, there is sample selectivity deviation. 2. When the parameters were measured, the solid part of the nodules was interfered with by cystic, blood and other components, which brought certain errors to the measurement results. 3. The optimal setting of the IVIM high b value needs to be further studied. In the future, combined with the dynamic enhancement of DCE in thyroid MRI, the correlation between the enhancement mode of lesions and the parameters under the IVIM theory can be further studied to bring more information and value to distinguishing between benign and cancerous thyroid nodules.

In conclusion, three techniques are significant in discriminating between benign thyroid nodules and PTC. MRI based on ZOOMit IVIM imaging has better diagnostic efficiency than ultrasonography and CT in differentiating PTC. However, this needs further research to verify.

ACKNOWLEDGMENTS

No funding or sponsorship was received for this study or publication of this article.

***Ethics approval and consent to participate*:** This study was conducted in accordance with the declaration of Helsinki.This study was conducted with approval from the Ethics Committee of Maanshan People's Hospital.Written informed consent was obtained from all participants.

***Competing Interest*:** The authors declare that they have no competing interests.

***Funding*:** He YS and Qi X Conception and design, Luo X and Wang WL Administrative support, Yang HK and Wu XY Provision of study materials or patients, XU M and Fan WJ Collection and assembly of data, He YS and Qi X ,Data analysis and interpretation. Manuscript writing and Final approval of manuscript: by the all authors.

***Availability of data and materials*:** All data generated or analyzed during this study are included in this published article.

REFERENCES

1. Chinese Society of Endocrinology, Chinese Medical Association Surgery Branch Endocrinology Group, China Anti-cancer Association, Chinese Society of Nuclear Medicine. (2013) Guidelines for diagnosis and treatment of thyroid nodules and differentiated thyroid carcinoma. *Chinese Journal of Nuclear Medicine and Molecular Imaging, **33**: 96-115*.
2. Chen F, Wu K, Xu MX, Yang Y (2017) Meta-analysis of risk factors for thyroid cancerbased on case-control studies. *Chinese Jouranl of Endemiology, **36**: 250-256*.
3. Lubitz CC and Sosa JA (2016) The changing landscape of papillary thyroid cancer: Epidemiology, management, and the implications for patients. *Cancer, **122**(24): 3754-3759*.
4. Lee CY, Kim SJ, Ko KR, *et al.* (2014) Predictive factors for extrathyroidal extension of papillary thyroid carcinoma based on preoperative sonography. *J Ultrasonography Med, **33**(2): 231-8*.
5. Lin Y, Lai S, Wang P, *et al.* (2022) Performance of current ultrasound-based malignancy risk stratification systems for thyroid nodules in patients with follicular neoplasms. *Eur Radiol, **32**(6): 3617-3630*.
6. Martens RM, Noij DP, Ali M, *et al.* (2019) Functional imaging early during (chemo)radiotherapy for response prediction in head and neck squamous cell carcinoma; a systematic review. *Oral Oncol, **88**: 75-83*.
7. Bonjoc KJ, Young H, Warner S, *et al.* (2020) Thyroid cancer diagnosis in the era of precision imaging. *J Thorac Dis, **12**(9): 5128-5139*.
8. Li M, Zheng X, Gao F, *et al.* (2016) Spectral CT imaging of intranodular hemorrhage in cases with challenging benign thyroid nodules. *Radiol Med, **121**(4): 279-290*.
9. Le Bihan D, Breton E, Lallemand D, *et al.* (1986) MRimaging of intravoxel incoherent motions: application to diffusion and perfusion inneurologic disorders. *Radiology, **161**(2): 401-7*.
10. Sim KC, Park BJ, Han NY, *et al.* (2020) Efficacy of ZOOMit coronal diffusion-weighted imaging and MR texture analysis for differentiating between benign and malignant distal bile duct strictures. *Abdom Radiol (NY), **45**(8): 2418-2429*.
11. Ai ZD, Hou J, Li FP, *et al.* (2017) Intravoxel incoherent motion diffusion weighted magnetic resonance imaging for differentiation between benign and malignant thyroid nodules. *Chinese Journal of Magnetic Resonance Imaging, **8**(10): 742-747*.
12. He ZZ, Zhou QQ, Yu YS, *et al.* (2020) Evaluation of thyroid gland image quality by conventional and ZOOMit DWI. *Chinese Computed Medical Imaging, **26**(4): 324-328*.
13. Tan H, Chen J, Xu QZ, *et al.* (2016) Differentiation of benign and

[DOI: 10.61186/ijrr.21.3.537]

malignant thyroid nodules using intravoxel incoherent motion. *Chinese Journal of Medical Imaging,* ***24****(3): 166-169, 174*.
14. Ito Y, Fujii K, Murase T, *et al.* (2017) Striated duct adenoma presenting with intra-tumoral hematoma and papillary thyroid carcinoma-like histology. *Pathol Int,* ***67****(6): 316-321*.
15. Rago T, Scutari M, Loiacono V, *et al.* (2017) Low elasticity of thyroid nodules on ultrasonography elastography is correlated with malignancy, degree of fibrosis, and high expression of Galectin-3 and Fibronectin-1. *Thyroid,* ***27****(1): 103-110*.
16. Liu PQ, Liu ZL, Wu KLg, *et al.* (2017) Value of SWE and real-time tissue elastography in the differential diagnosis of benign and malignant thyroid nodules. *Chinese Journal of Operative Procedures of General Surgery, (Electronic Edition)*, ***11****(05): 393-396*.
17. Ao LJ and Liu YL (2020) Application value of shear wave elastography in differential diagnosis of benign and malignant thyroid nodules. *Journal of Diseases Monitor and Control,* ***14****(02): 89-93*.
18. Han ZJ, Lei ZK, Chen WH, Luo DC (2014) Value of sonography and CT in the preoperative evaluation of cervical lymph node metastasis for papillary thyroid carcinoma. *Journal ofChina Clinic Medical Imaging,* ***25****(11): 804-806*.
19. Gao SY, Zhang XY, Wei W, *et al.* (2016) Identification of benign and malignant thyroid nodules by in vivo iodine concentration measurement using single-source dual energy CT: A retrospective diagnostic accuracy study. *Medicine, (Baltimore)* ***95****(39): e4816*.
20. Seidler M, Forghani B, Reinhold C, *et al.* (2019) Dual-energy CT texture analysis with machine learning for the evaluation and characterization of cervical lymphadenopathy. *Comput Struct Biotechnol J,* ***17****: 1009-1015*.
21. Li L, Wang Y, Luo DH, *et al.* (2017) Diagnostic value of single-source dual-energy spectral computed tomography for papillary thyroid microcarcinomas. *J Xray Sci Technol* ***25****(5): 793-802*.

[DOI: 10.61186/ijrr.21.3.537]